Powder Technology 407 (2022) 117691

Contents lists available at ScienceDirect

Powder Technology

journal homepage: www.journals.elsevier.com/powder-technology

Photothermal and recycling properties of new composite magnetic nanofluids

Zhibo Tang, Lanqi Chen, Cong Qi *, Zhen Tian

School of Low-carbon Energy and Power Engineering, China University of Mining and Technology, Xuzhou 221116, China

HIGHLIGHTS

- Fe_3O_4 particles are decorated on CNTs to form new composite nanoparticles.
- The collection efficiency of DASC can reach 94.14%.
- Fe_3O_4/CNTs nanoparticles have good recoverability and recycling properties.
- Lower nanofluids depth is beneficial to improving heat collection efficiency.

GRAPHICAL ABSTRACT

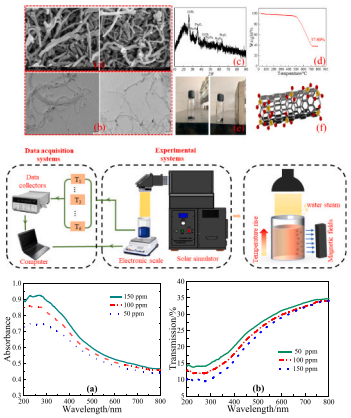

ARTICLE INFO

Keywords:
Photothermal conversion
Nanofluids
Direct absorption collector
Carbon nanotube

ABSTRACT

The efficient conversion of solar energy is beneficial to reducing energy consumption. To improve the photothermal efficiency of direct absorption photothermal conversion system, Fe_3O_4 particles are decorated on the carbon nanotube particles through chemical co-sedimentation to prepare new composite magnetic Fe_3O_4/CNTs nanofluids, which have good paramagnetic properties under the action of magnetic field and show good photothermal efficiency. Photothermal conversion, recovery and recycling experiments of composite magnetic nanofluids were conducted. The effects of nanofluids concentration, illumination intensity, and nanofluids depth on the photothermal efficiency were investigated. Results indicated that there is a critical concentration, beyond which there is no significant increase in photothermal efficiency. Besides, the increase of nanofluids depth will increase the heat loss inside the nanofluids, which is not conducive to photothermal absorption. Meanwhile, under the action of magnetic field, Fe_3O_4/CNTs nanofluids show good recoverable performance, and the stable photothermal efficiency can still be maintained after several cycles.

* Corresponding author.
E-mail address: qicong@cumt.edu.cn (C. Qi).

https://doi.org/10.1016/j.powtec.2022.117691
Received 25 March 2022; Received in revised form 13 May 2022; Accepted 29 June 2022
Available online 4 July 2022

Nomenclature

A	irradiated area, m^2
B	magnetic field intensity, mT
c	specific heat, J/(kg·k)
G	illumination intensity, w/m^2
h_{lv}	latent heat of vaporization, kJ/kg
m	total nanofluid mass, kg
m_{nf}	nanofluids mass, kg
m_c	quality of dried nanoparticles, kg
m_e	surface evaporation mass of water, kg/m^2
m_w	equivalent surface mass of the remaining nanofluids, kg/m^2
Q_{in}	heating power, kW
Q_{lh}	total heat of water evaporation, kW
Q_{net}	effective heating power, kW
Q_{loss}	heat loss, kW
T	temperature, °C
T_f	initial temperature, °C
T_i	ending temperature, °C

Greek symbols

η	heating efficiency
η_t	heat collection efficiency
η_c	recovery efficiency
Δ	difference

Subscript

nf	nanofluids

1. Introduction

Since the industrial revolution, along with the speedy progress of industrial technology, the consumption of traditional energy sources has been increasing, and energy shortage and environmental pollution have become another major challenge for mankind. Searching clean energy sources and developing technologies to use it effectively play a crucial role in solving energy problems. Solar energy is widely distributed, green and non-polluting, and has a huge amount of energy to solve the problem of resource scarcity that people face, making it one of the most ideal green energy sources [1]. In recent years, nanofluids have shown excellent properties as a new working medium for solar energy absorption [2]. As a working fluid with excellent thermodynamic properties [3,4], properties of nanofluids such as thermal conductivity [5,6], viscosity [7] and interfacial properties [8] have been studied extensively. Nanofluids are also used by a large number of scholars in various industrial applications such as natural convection [9,10], forced convection [11,12], boiling heat transfer [13,14], heat pipe [15,16], microchannel [17,18], photothermal conversion [19], and so on. Nanofluids show excellent application prospects as a new solar energy utilization workpiece.

In general, photothermal conversion is a direct and efficient way to convert solar energy into thermal energy, and in recent years, a lot of research has been conducted on direct absorption photothermal conversion systems using nanofluids as the base fluid. Chen et al. [20,21] prepared Ag nanoparticles and experimentally investigated their photothermal conversion properties. The experimental results showed that the photothermal conversion performance of Ag nanofluids is nearly double that of pure water and also much larger than that of ZnO nanofluids. Jeon et al. [22] characterized the optical properties of gold nanorod nanofluids with various aspect ratios. The tunability of Au nanoparticles in infrared and visible light is proved. The calculation showed that the ideal extinction coefficient can be obtained when the length of nanorods is 72 nm. Yu et al. [23] based on the seed growth method, prepared gold nanostars with different tip numbers and sharpness by controlling the proportion of auxiliary reagent $AgNO_3$, experimental results showed that gold nanostars with larger tip length and sharpness have higher photothermal conversion efficiency. Xuan et al. [24] prepared TiO_2/Ag composite nanofluids by photochemical impregnation method and verified the photothermal properties. The results showed that TiO_2/Ag composite nanofluids have a higher photothermal conversion temperature than pure TiO_2 nanofluids. Li et al. [25–27] successfully synthesized Ag@TiO_2 core-shell structure nanoparticles by the one-step method using DMF as the reducing agent of Ag^+ and carried out the experimental evaluation of photothermal and photoelectric properties. The photothermal evaporation experiment showed that compared with water, the photothermal evaporation efficiency of Ag@TiO_2 increases from 14.2% to 53.9% under 5 sun. Huang et al. [28] prepared Au@TiO_2 nanoparticles by hydrothermal method and prepared microporous Au@TiO_2 composite film by vacuum extraction and filtration method for water evaporation experiment. The experimental results showed that the core-shell structure can significantly enhance the photothermal conversion efficiency due to a wider absorption spectrum, and the effect is higher than that of pure Au, TiO_2, and Au-TiO_2 mixed films, reaching 49.65%.

Compared with precious metals, carbon-based materials are easy to prepare, cheap, and readily available. The carbon-based nanofluids are black and have a strong light absorption capacity. They convert solar energy into thermal energy through lattice vibration, have good stability, optical and thermal properties, and are excellent working medium for photo-thermal absorption [29]. Common carbon-based nanomaterials include graphite nanoparticles [30], carbon nanotubes [31], carbon layer metals [32] and carbon nanohorns [33], and so on. Carbon-based materials can be regarded as a large π bond conjugated system, requiring only a small input of energy to excite relaxed electrons from π orbital to π* orbital. When the electrons are excited from the ground state to a higher energy orbital, the electrons relax back to the ground state and release heat to complete the photothermal transformation. In the field of photothermal conversion, carbon-based materials show great competitiveness in terms of cost, stability, high thermal conductivity, and scalability. The first application of carbon nanotubes as the absorbent medium in a direct absorption solar collector (DASC) was made by Karami et al. [34] The findings indicated that the extinction coefficient and heat conductivity of the nanofluids can be significantly improved even at lower mass fractions. Chen et al. [35] prepared reduced graphene oxide (RGO) nanofluids using the UV irradiation method. It was shown that the RGO/water nanofluids could achieve high photothermal conversion efficiency up to 96.93% at a low-temperature atmosphere. Hordy et al. [36] reported glycol-based multi-walled carbon (MWCNT) nanotube nanofluids for DASC, confirming their long-term room temperature stability and high spectral absorption. Chen et al. [37] used SiC dispersed in ionic liquids to improve the optical and thermal properties of nanofluids, and the results showed that SiC/ionic liquids exhibits the best performance in the medium and high-temperature systems. Gorji et al. [38] investigated the photothermal conversion characteristics of graphite, magnetite, and silver as working medium. The results showed a more uniform temperature distribution within the collector at lower concentrations. Li et al. [39] modified carbon nanotubes with β-cyclodextrin which have good hydrophilic and optical properties. The results showed that the extinction coefficient of nanofluids can be improved by 4.3 cm^{-1} when the volume fraction is 0.01 vol%. Liu et al. [40] used the modified graphene dispersed in [HMIM]BF4 base solution as the working solution of DASC. The experimental results showed that the GE/[HMIM]BF4 nanofluids have great thermal storage capacity and

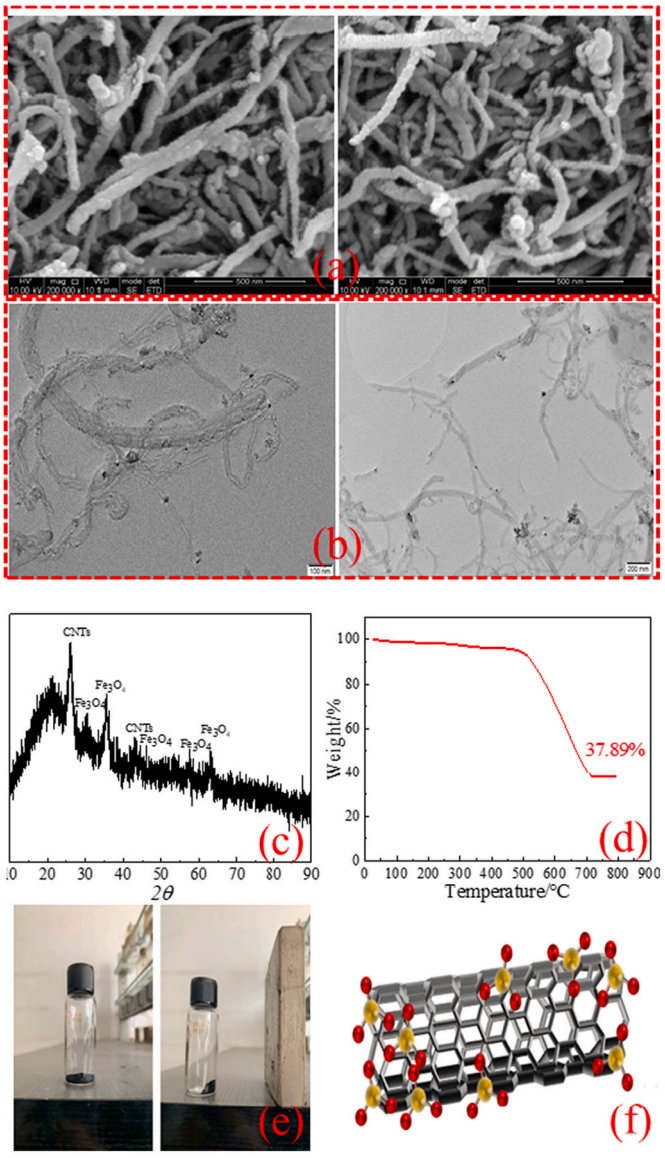

Fig. 1. Characteristics of Fe_3O_4/CNTs. (a) SEM, (b) TEM, (c) XRD, (d) TGA (e) Magnetic properties of Fe_3O_4/CNTs, (f) Schematic of the modifications,

exhibit good dispersion stability at high temperatures. Mashhadian et al. [41] investigated the photothermal performance of Al_2O_3/MWCNTs hybrid nanofluids in a collector. The experimental findings indicated that the use of hybrid nanofluids increases the thermal efficiency of solar collectors by 197.1% compared to water. Struchalin et al. [42] experimentally investigated the thermal efficiency of Fe_3O_4/MWCNT hybrid nanofluids for DASC. The research findings indicated that the thermal efficiency of DASC using hybrid nanofluids ranges from 52.3 to 69.4%. Delfani et al. [43] investigated the effect of volume fraction and height of MWCNT nanofluids on the photothermal performance of DASCs. The results showed that the DASC collection efficiency is increased by 10–29% compared to the base fluid. Tong et al. [44] investigated the thermal properties of MWCNT nanofluids inside U-tubes. The results showed that the efficiency is increased by 4% after using MWCNTs. Kasaeian et al. [45] compared the thermal efficiency of MWCNT/EG and SiO_2/EG nanofluids in solar collectors. The results showed that the highest thermal efficiency is achieved when the volume fraction of MWCNT/EG is 0.3%, which is 17% higher than that of the base fluid.

As described in the literature above, a great number of researchers have investigated the photothermal applications of noble metals, carbon nanotubes, and hybrid nanofluids indirect absorption solar collectors. However, all of the above photothermal materials are characterized by expensive costs and difficulties in recycling. Fewer scholars have studied functionalized nanofluids and focused on their recycling. Therefore, in the present work, functionalized carbon nanotubes loaded with Fe_3O_4 were prepared and the photothermal performance of Fe_3O_4/CNTs nanofluids indirect absorption solar collectors was investigated. The novelties of this paper are as follows: First, different from the previous direct mixing of two nanoparticles to prepare the hybrid working fluid, in this paper, Fe_3O_4 particles are decorated on carbon nanotube particles through chemical co-sedimentation. The functionalized nanofluids of Fe_3O_4/CNTs were prepared and characterized in terms of morphology and optical properties. Second, a direct absorption photothermal conversion experimental bench was built to investigate the effects of nanofluids concentration, solar radiation intensity, and collector depth on photothermal performance. Finally, the effects of different magnetic field strengths on the nanofluids' recovery efficiency were investigated. This paper provides guidance on ideas for developing novel functionalized nanofluids for photothermal conversion applications.

2. Materials and experiments

2.1. Nanofluids and characterization

2.1.1. Synthesis of Fe_3O_4/CNTs

In this work, Fe_3O_4/CNTs were prepared by the chemical co-sedimentation method. In the co-precipitation method, NaOH was used as a precipitant, and Fe^{3+} and Fe^{2+} reacted according to Eq. (1) to nucleate on the surface of carbon nanotubes, and finally formed Fe_3O_4 nanoparticles. First, the carbon nanoparticles were placed in a tube furnace and calcined in a 600 °C atmosphere for 5 h. Then, 5 g of carbon nanotubes were added into 100 ml of concentrated HCl and sonicated for 1 h to make the carbon nanotubes fully dispersed in the solution.

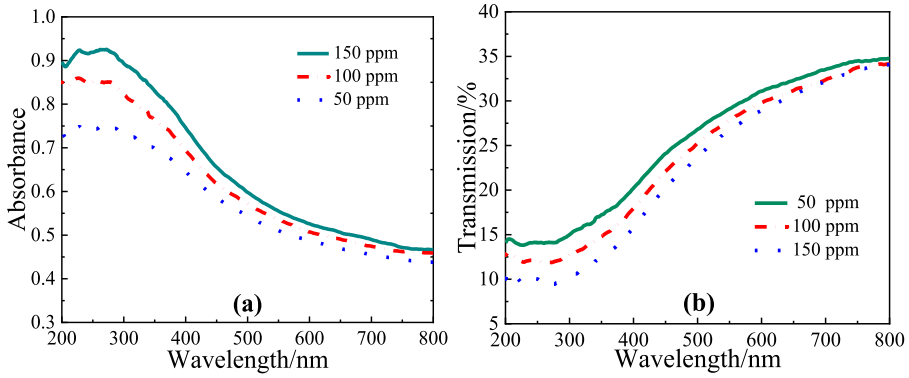

Fig. 2. Absorbance and transmittance of Fe_3O_4/CNTs nanofluids. (a) Absorbance, (b) Transmittance.

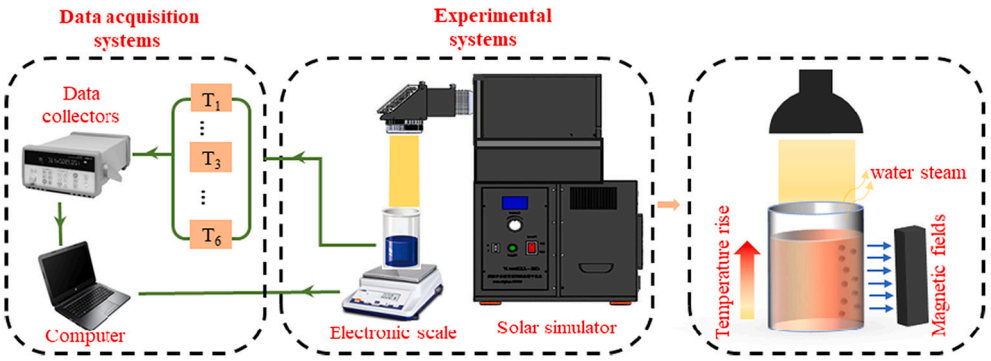

Fig. 3. Schematic diagram of the experimental system.

Table 1
Uncertainties of parameters.

Variables	*m*	*T*	*G*	*A*
Uncertainty	±0.3%	±0.1%	±5.0%	±1.21%

After acidification, the solution was filtered to neutral. The filtered CNTS was dried in a vacuum drying oven. Then carbon nanotubes loaded with Fe_3O_4 were prepared. Solution A was first prepared by adding 1 g of CNTs to 100 ml of deionized water, and sonicating for 30 min. Take 1.353 g of $Fecl_3$-$6H_2O$ and 0.695 g of $FeSO_4$-$7H_2O$ and add 250 ml of deionized water to configure solution B. Solution A and solution B were mixed in a three-necked flask, heated to 55 °C in an oil bath with mechanical stirring and reacted for 30 min. The solution in the three-mouth flask was warmed to 65 °C and NaOH solution was added dropwise to pH > 12 and reacted for 1 h. The solution was continued to be warmed up to 80 °C, 0.25 g of SDS ($CH_3(CH_2)_{11}OSO_3Na$) was added and cooled to room temperature under mechanical stirring. Finally, the above solution was washed by filtration to neutral and dried in a vacuum drying oven. The carbon nanotubes used in this work were provided by Chengdu Institute of Organic Chemistry, Chinese Academy of Sciences, with a purity of >98% and a specific surface area of 380–550 m^2/g.

$$2Fe^{3+} + Fe^{2+} + 8OH^- \rightarrow Fe_3O_4 + 4H_2O \quad (1)$$

In this work, nanofluids were prepared by mechanical stirring and ultrasonic vibration. First, the nanoparticles prepared above were dissolved in deionized water and mixed with mechanical stirring. Then, the mixed nanofluids were ultrasonically shaken for 20 min, so that the nanoparticles were uniformly dispersed in the water. When the concentration of the nanofluids is 150 ppm, the optical path of light in the solution is small, and it is not meaningful to increase the concentration of the solution to capture light. Therefore, nanofluids with concentrations of 50–150 ppm were prepared in this paper.

2.1.2. Characterization

SEM and TIM were used to observe the morphology of Fe_3O_4/CNTs. It can be seen from the SEM and TIM images (Fig. 1) that the Fe_3O_4 nanoparticles are uniformly attached to the tubular CNTs. The elemental composition and lattice structure of Fe_3O_4/CNTs were confirmed by means of using X-ray diffraction characterization, and the results are shown in Fig. 1(c). It is obvious from Fig. 1(c) that distinct characteristic peaks appear at two positions $2\theta = 25.7°$ and 42.8°, corresponding to the (002) and (100) crystalline structures. From the six characteristic peaks at 2θ = 30.6°, 35.4°, 43.1°, 57.1°, and 62.6° corresponding to (220), (311), (400), (511), and (440) spinel crystalline facets, it can be concluded that Fe_3O_4 is a spinel structure (JCPDS No.19–629). Fig. 1(d) shows the TGA characterization curve. The test conditions are from room temperature to 800 °C, and the heating rate is 20 °C/min. It can be seen that within the experimental temperature range of this paper, Fe_3O_4/CNTs exhibit good thermal stability. It is clear from Fig. 1(e) that the prepared Fe_3O_4/CNTs have obvious paramagnetic properties. Fig. 2 shows the absorbance and transmittance of the nanofluids. It is clear to see that the nanofluids have a high absorbance and low transmittance in the visible range, which has a strong light trapping ability.

2.2. Photothermal conversion experiment

The schematic diagram of the photothermal conversion experiment is shown in Fig. 3. The photothermal conversion experiment is divided into three main parts. One part is the simulated light system. The light source is provided by a xenon light source that simulates sunlight. In daily life, the intensity of sunlight generally does not exceed 5 sun. Therefore, in this paper, 2–6 sun light intensity is chosen to carry out the light experiment. Another part is the heating and evaporation system, the size of the heating chamber is 40 × 40 × 50 mm, the thickness is 3

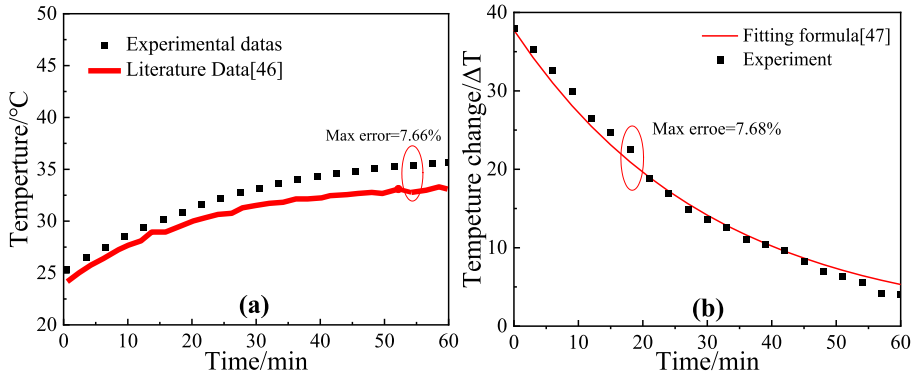

Fig. 4. Validation of the experimental system. (a) Temperature of water, (b) Temperature change after illumination.

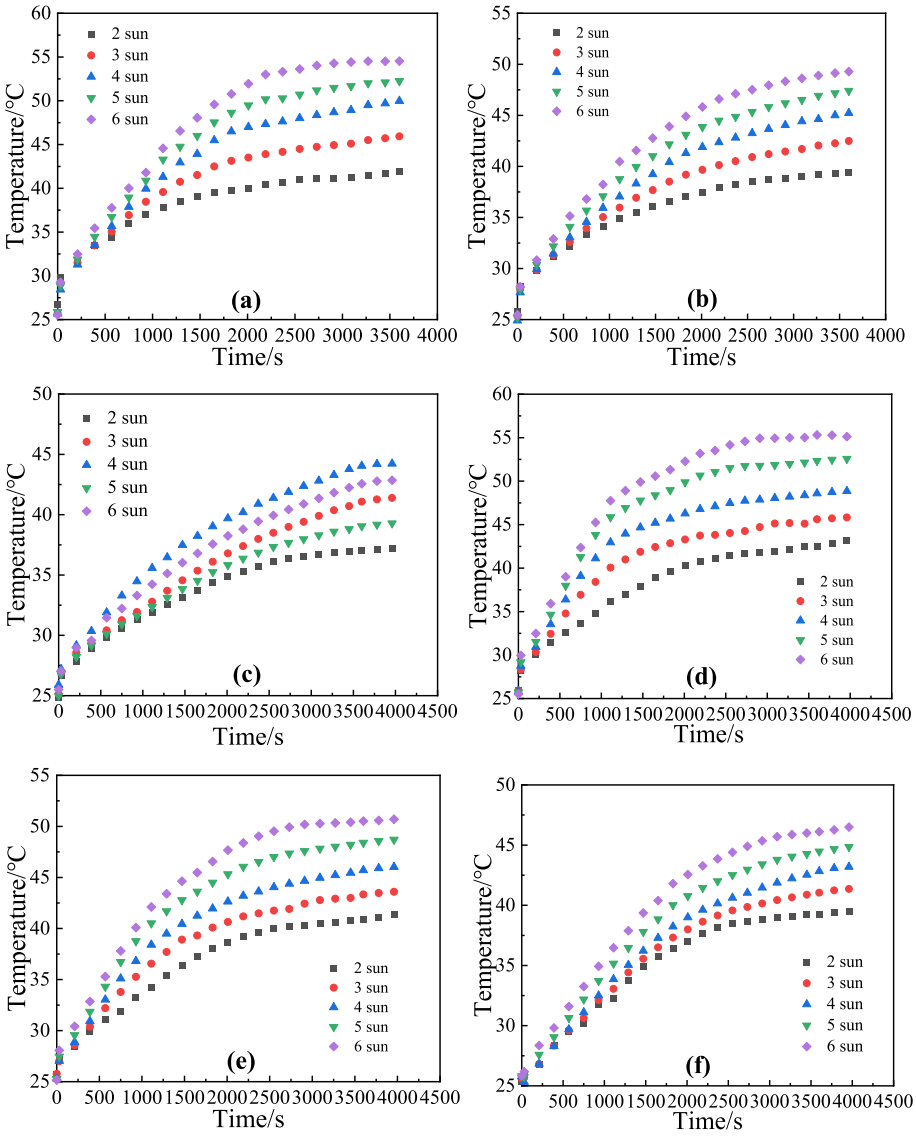

Fig. 5. Temperature rise of nanofluids with different mass fraction at different depths. 50 ppm: (a) 20 mm, (b) 30 mm, (c) 40 mm; 100 ppm: (d) 20 mm, (e) 30 mm, (f) 40 mm; 150 ppm: (g) 20 mm, (h) 30 mm, (i) 40 mm, (j) water, 30 mm.

mm. The material of the heating chamber is the acrylic plate, and its interior is filled with the corresponding nanofluids. To prevent light loss, a layer of commercial black graphene sheet is attached to the inside of the heating wall to absorb the overflowing sunlight. The third part is the data collection system, six thermocouples are evenly distributed inside the heated chamber to record the temperature of the nanofluids inside the chamber. The thermocouples are located in the middle of the side of the cavity, and the distance between each thermocouple is 3 mm, which is evenly distributed from top to bottom. The chamber is placed on a precision balance and the change in nanofluids mass is recorded at regular intervals. Finally, the experimental data are collected on the computer.

2.3. Experiment performance evaluation

The heating efficiency η can be evaluated by Eq. (2).

$$\eta = \frac{Q_{nf}}{Q_{in}} = \frac{m_{nf} c_{nf} \Delta T}{AG\Delta t} \tag{2}$$

where Q_{nf} is the energy of the temperature rise of the nanofluids and Q_{in} is the total energy incident to the system; m_{nf} is the nanofluids mass; c_{nf} is the specific heats of the nanofluids, ΔT is the temperature difference; A is the irradiated area; G is the irradiation intensity.

The heat collection efficiency η_t can be calculated by Eq. (3).

$$\eta_t = \frac{Q_{nf} + Q_{lh}}{Q_{in}} = \frac{m_w c_{nf} \Delta T + \Delta m_e h_{1v}}{G\Delta t} \tag{3}$$

where Q_{lh} is the latent heat of vaporization of water evaporation; Δm_e is the surface evaporation mass of water in a certain time; m_w is the equivalent surface mass of the remaining nanofluids; h_{lv} is the latent heat of vaporization at standard atmospheric pressure.

The recovery efficiency η_c can be evaluated by Eq. (4).

$$\eta_c = \frac{m_c}{m} \tag{4}$$

where m_c is the recovering the quality of dried nanoparticles.

2.4. Uncertainty analysis

The measurement error of each physical parameter will make a large

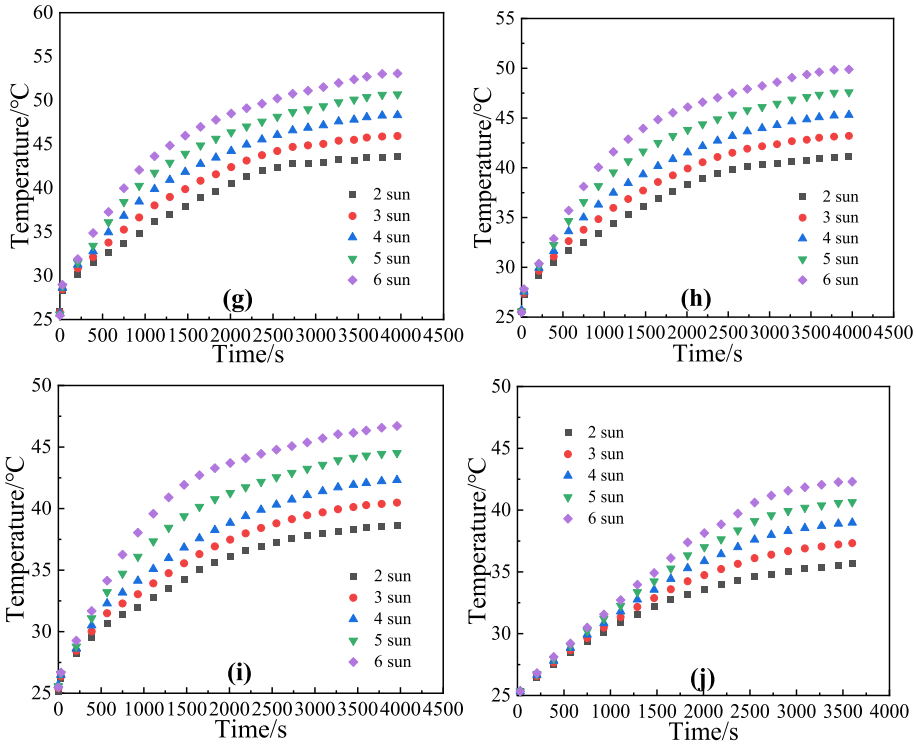

Fig. 5. (*continued*).

influence on the results. To ensure the reliability of the data, a corresponding error analysis is essential. The relative error E_η and $E\eta_t$ are calculated by Eq. (5) and Eq. (6), respectively.

$$E_\eta = \sqrt{\left(\frac{\sigma m_{nf}}{m}\right)^2 + \frac{\sigma_{Tf}^2 + \sigma_{Ti}^2}{\left(T_f - T_i\right)^2} + \left(\frac{\sigma_A}{A}\right)^2 + \left(\frac{\sigma_G}{G}\right)^2} \tag{5}$$

$$E_{\eta_t} = \sqrt{\left(\frac{\sigma m_w}{m}\right)^2 + \frac{\sigma_{Tf}^2 + \sigma_{Ti}^2}{\left(T_f - T_i\right)^2} + \left(\frac{\sigma m_e}{m}\right)^2 + \left(\frac{\sigma_G}{G}\right)^2} \tag{6}$$

In this work, the uncertainties of each parameter are shown in Table 1. The maximum uncertainty errors for η and η_t are 5.15% and 5.01%, respectively, which are within acceptable limits.

2.5. Experimental system verification

To verify the credibility of the experimental system, the results of this work were compared with data and empirical formulas from similar literature [46,47], and the results are displayed in Fig. 4. From Fig. 4, it is clear to see that the maximum errors are 7.66% and 7.68%, respectively, thus proving that the experimental system is reliable.

3. Result and discussion

3.1. Effect of concentration of nanofluids

3.1.1. Temperature rise characteristic

In this part, the effect of the concentration of nanofluids on the temperature rise characteristics of the solar collector is analyzed. Fig. 5 (a)(d)(g), (b)(e)(h) and (c)(f)(j) show the temperature rise variation of the collector under different nanofluids concentration conditions, respectively. From Fig. 5(a), it is clear to see that when the concentration is 50 ppm, the maximum temperature rise can be increased by 17.46–28.89% compared to deionized water. This is since nanoparticles greatly reduce the spectral transmittance of the nanofluids compared to deionized water, allowing the collector to greatly increase its ability to capture sunlight. That is, the addition of nanoparticles will result in enhanced scattering and absorption of light in the nanofluids, thereby increasing the optical path. Meanwhile, it is clear to see that Fig. 5(d), (g) that the maximum temperature rise can be increased by 20.98–29.81% and 22.13–25.43% when the mass fraction is increased to 100 ppm and 150 ppm respectively under the same depth conditions. It is clear to see that as the nanofluids concentration increases, the spectral transmittance of the nanofluids is further reduced, thus increasing the temperature rise ratio of the collector. However, increasing the concentration of nanofluids is not always beneficial, and the temperature rise ratio decreases when the concentration increases to 150 ppm. This is because a larger nanofluids concentration does not allow light to penetrate the nanofluids, thus increasing the nanofluids' longitudinal temperature difference and thus decreasing the temperature rise ratio.

Fig. 6 gives the variation of the heating efficiency of the nanofluids inside the collector with time. It is clear to see that the heating efficiency gradually decreases with the increase of light time. In this paper, the heating efficiency is defined as the ratio of sensible heat required to increase the temperature of the nanofluids to the total energy input to the system. At the early stage of illumination, only a small portion of the heat in the collector is used for water evaporation, and most of the energy is used for nanofluids temperature increase, resulting in a higher heating efficiency at the early stage of illumination, while with the increase of illumination time, part of the energy is used to provide the latent heat of vaporization required for water evaporation, so the heating efficiency decreases, which is consistent with the thermodynamic law. Meanwhile, Fig. 6 shows the heating efficiency increases in all periods when the concentration increases from 50 ppm to 100 ppm, while there is almost no increase in the heating efficiency when the concentration increases from 100 ppm to 150 ppm, which is consistent with the heating temperature law in the upper part.

3.1.2. Water evaporation characteristics

In this part, the effect of the mass fraction of nanofluids on the water evaporation characteristics of the solar collector is analyzed. From Fig. 7

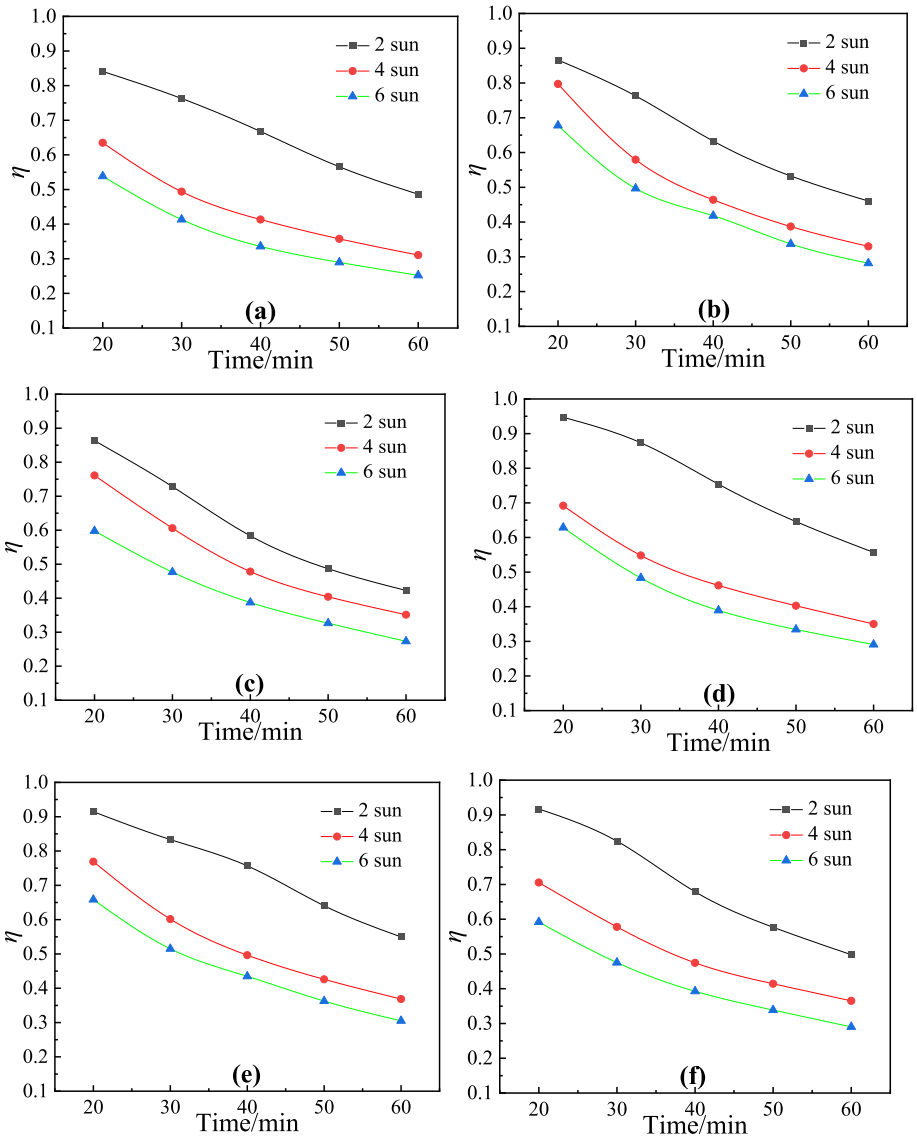

Fig. 6. Heating efficiency of nanofluids with different mass fraction at different depths. 20 mm: (a)150 ppm, (b) 100 ppm, (c) 50 ppm; 30 mm: (d) 150 ppm, (e) 100 ppm, (f) 50 ppm; 40 mm: (g) 150 ppm, (h) 100 ppm, (i) 50 ppm, (j) water, 30 mm.

(a), it is clear to see that when the nanofluids mass fraction is 50 ppm, the evaporated mass can be increased by 44.17–56.09% compared to deionized water. As seen in Fig. 7(d) and (g), the evaporated mass can be increased by 54.95–67.59% and 58.63–69.29% when the mass fraction is increased by 100 ppm and 150 ppm, respectively. Similar to the temperature rise variation, the first increase in evaporated mass tends to level off as the nanofluids mass fraction increases. The reasons for this situation are the same as in the previous section. From Fig. 7(b) and (c), it is clear to see that the evaporated mass can be increased by a maximum of 47.78% and 39.42% at a mass fraction of 50 ppm when the collector depth is 30 mm and 40 mm, respectively. From Fig. 7(e) and (f), there is a large increase in the mass increase rate when the mass fraction is increased to 100 ppm, and the evaporated mass can be increased by 60.22% and 55.12% at maximum. While by Fig. 7(h) and (i), there is no significant increase in the mass increase rate, and the maximum increase is only 61.11% and 58.33%.

The photothermal evaporation rates of nanofluids at different concentration conditions are displayed in Fig. 8. When the concentration is from 50 ppm, the evaporation rate reaches a maximum value of 1.422 $kg{\cdot}m^{-2}{\cdot}h^{-1}$ when the light intensity is 6 sun. Under the same conditions, when the mass fraction is increased to 100 ppm, the evaporation rate can be up to 2.25 $kg{\cdot}m^{-2}{\cdot}h^{-1}$.

3.1.3. *Heat collection efficiency*

The variation of the heat collection efficiency of the collectors for different concentration conditions is given in Fig. 9. In this paper, the heat collection efficiency is defined as the ratio of the sum of the sensible heat (required to increase the temperature of the nanofluids and the latent heat required to evaporate the water vaporization) to the total energy input to the system. The collector efficiency provides a comprehensive evaluation of the solar thermal conversion performance of a solar collector. When the collector depth is 20 mm, the collector efficiency of the solar collector increases from 68.64% to 77.24% as the concentration increases from 50 ppm to 100 ppm. While when the concentration continued to increase to 150 ppm, the collector efficiency decreases to 74.15% instead. Fig. 9 shows that when the concentration of nanofluids is low, increasing the concentration of nanofluids appropriately helps to improve the efficiency of the collector in using sunlight, while when the concentration of nanofluids is in the higher range, continuing to increase the concentration is not always beneficial to the

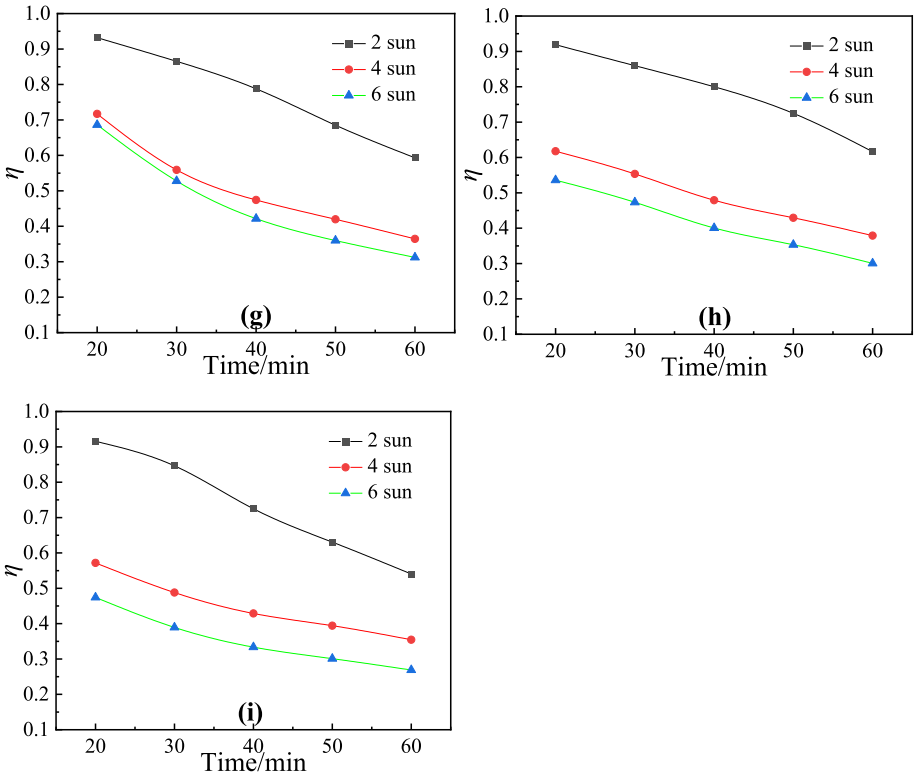

Fig. 6. (*continued*).

efficiency of the collector. There exists a critical concentration range that allows the solar collector to collect.

3.2. Effect of illumination intensity

3.2.1. Temperature rise characteristic

The variation of the temperature rise of the nanofluids with the light intensity under different working conditions is given in each subplot of Fig. 5. The temperature of the nanofluids increases with the increase of light intensity. As shown in Fig. 5(a), when the solar intensity is raised from 2 sun to 6 sun, the temperature of the nanofluids can be increased by 6.23–12.78 °C compared to that of deionized water. Similarly, increasing the light intensity at a concentration of 100 ppm increases the nanofluids' temperature by 10.39–13.86 °C compared to deionized water, as shown in Fig. 5(d)–(f). This is due to the optical properties of the nanoparticles themselves that improve the ability of the nanofluids to capture light, thus increasing the temperature of the nanofluids as the light intensity increases and the collector is able to collect more energy.

Fig. 6 indicates the influence of nanofluids' depth on the heating efficiency of the collector under different operating conditions. It is clear to see that a smaller light intensity achieves greater heating efficiency, and as the light intensity increases, the heating efficiency decreases instead. The reason is that only a small fraction of the total solar energy entering the system is used to increase the sensible heat of the nanofluids, while most of the energy is used to provide the latent heat required for water evaporation and is lost to the environment, thus exhibiting a lower heating efficiency.

3.2.2. Water evaporation characteristics

Fig. 7 shows the mass change of the nanofluids under different light intensity conditions. The evaporation of water in the collector has a large increase with the augment of light intensity. As shown in Fig. 7(a)–(c), when the mass fraction of nanofluids is 50 ppm, the mass of water evaporated in the collector increases by 81.53–83.21% when the light intensity increases from 2 sun to 6 sun. Also similarly, when the mass fraction is 100 ppm and 150 ppm, the evaporated mass can be increased by 79.75–84.73%, as displayed in Fig. 7(d)–(i).

Fig. 8 indicates the variation of the evaporation rate of water inside the collector with the light intensity. As shown in Fig. 8, the evaporation rate of water rises with the increase of light intensity. When the light intensity is 2 sun, the evaporation rate is 0.282 $kg{\cdot}m^{-2}{\cdot}h^{-1}$, while when the light intensity increases to 6 sun, the evaporation rate can reach 1.422 $kg{\cdot}m^{-2}{\cdot}h^{-1}$, as shown in Fig. 8(a). Similarly, when the concentration was 100 ppm and 150 ppm, respectively, the evaporation rates could reach 2.25 $kg{\cdot}m^{-2}{\cdot}h^{-1}$ and 2.28 $kg{\cdot}m^{-2}{\cdot}h^{-1}$ under the same conditions, respectively.

3.2.3. Heat collection efficiency

Fig. 9 indicates the variation of the collector efficiency of the solar collector with the light intensity. It can be seen that the collector efficiency has more greater collector efficiency at lower light intensities, and the collector efficiency decreases slightly with the increasing light intensity. The maximum collector efficiency of solar collectors is achieved when the light intensity is 2 sun, reaching 93.33–94.92% at different mass fractions. This is since the increase in the energy used by the collector to heat the nanofluids and evaporate the water is less than the energy of the light, and more energy is lost in the environment, resulting in a lower collector efficiency.

3.3. Effect of depth of nanofluids

3.3.1. Temperature rise characteristic

From Fig. 5(a)(b)(c), (d)(e)(f), and (g)(h)(i), the effects of different collector depths on the nanofluids temperature rise at the same concentration can be compared. From Fig. 5(a)–(c), it is clear to see that at the same concentration, the slope of the collector temperature rise becomes smaller with the increasing depth and it takes longer time to reach higher temperatures. This is due to the fact that as the depth increases and the mass of the nanofluids increases and more energy is required to raise the same temperature, also the heat loss in nanofluids increases due

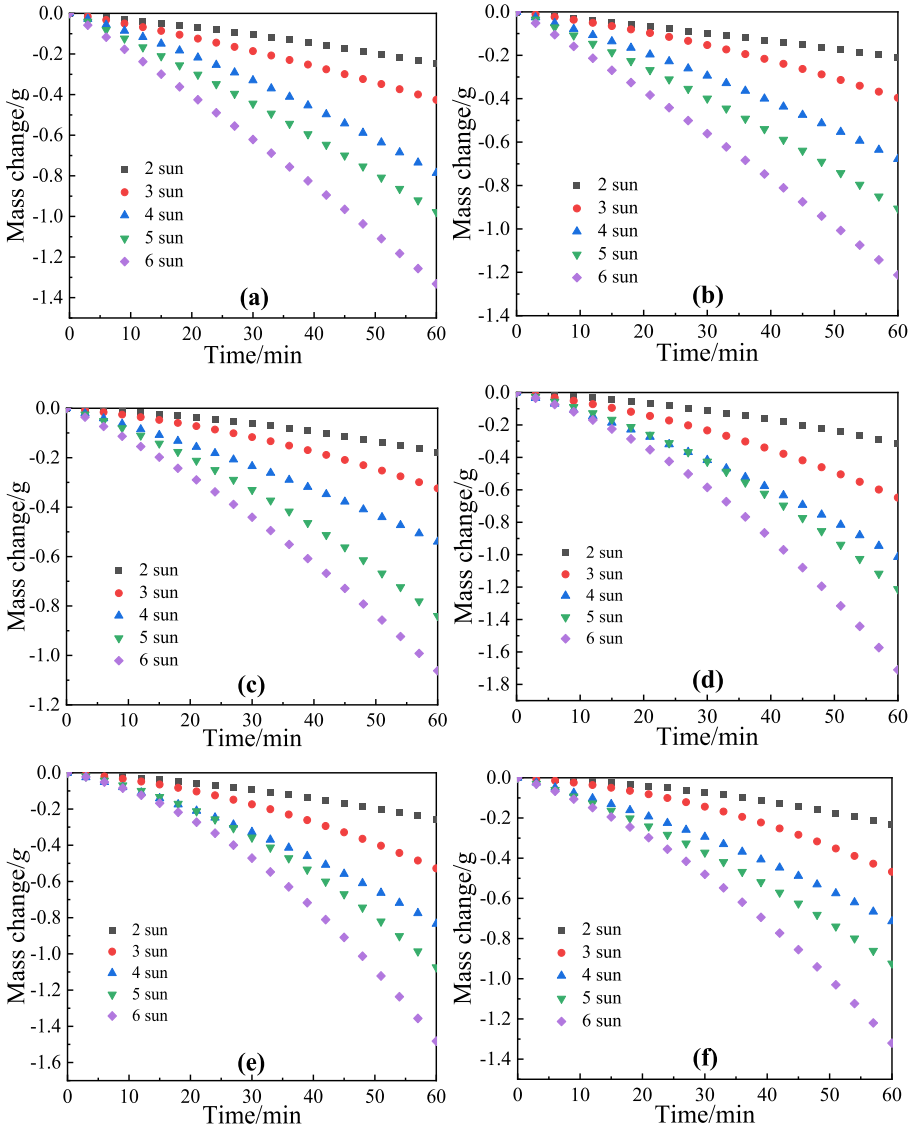

Fig. 7. Mass change of nanofluids with different mass fraction at different depths. 50 ppm: (a) 20 mm, (b) 30 mm, (c) 40 mm; 100 ppm: (d) 20 mm, (e) 30 mm, (f) 40 mm; 150 ppm: (g) 20 mm, (h) 30 mm, (i)40 mm, (j) water, 30 mm.

to the temperature difference inside the depth increase. Therefore, the maximum temperature that can be reached decreases as the depth increases at the same time. When the depth is 20 mm, the maximum collector temperature can reach 54.91 °C, which is 29.81% higher than that of deionized water under the same conditions. Similarly, when the depth is 30 mm and 40 mm respectively, the maximum temperature rise can be increased by a maximum of 19.86% and 10.82% respectively compared to deionized water.

The variation of heating efficiency with time for different collector depth conditions is given in Fig. 6. The variation of heating efficiency with time for different collector depth conditions is given in Fig. 6. When the collector depth is 20 mm, the heating efficiency can reach 25.22–48.63% after the light time reaches 60 min, as shown in Fig. 6(a)–(c). Similarly, when the depth is 30 mm and 40 mm, the heating efficiency can reach 29.03–55.71% and 26.90–59.32%, respectively. It can be seen that unlike the temperature rise variation, although the increase in depth decreases the maximum temperature rise reached in a certain time, the total amount of energy absorbed by a larger collector depth is greater, thanks to the equal large nanofluids mass. This provides a different reference standard for measuring the thermal performance of the collector.

3.3.2. *Water evaporation characteristics*

Fig. 7 indicates the change of the evaporated mass of water inside the collector with the depth of the nanofluids. It can be seen that at the same light intensity, the evaporation of water decreases with increasing depth, which is since a larger nanofluids depth increases the temperature inhomogeneity inside the nanofluids thus increasing the heat loss and causing a decrease in the evaporation mass. Fig. 8 indicates the variation of the evaporation rate of water inside the collector with depth. It can be seen that a smaller nanofluids depth has a greater evaporation rate for the same light intensity, which is consistent with the law of mass change.

3.3.3. *Heat collection efficiency*

Fig. 9 indicates the change of the collector efficiency of the solar collectors for different depth conditions. From Fig. 9, it can be seen that the collector efficiency can reach 77.24–94.14% when the nanofluids concentration is 100 ppm and the depth is 20 mm. With the increasing depth, the collector efficiency decreases due to the fact that greater

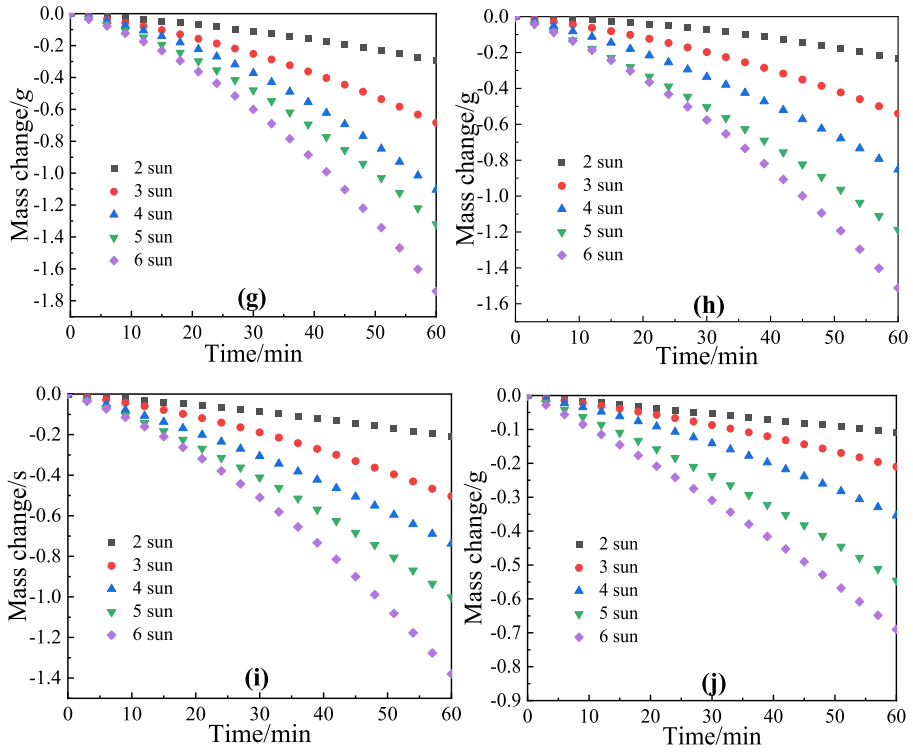

Fig. 7. (*continued*).

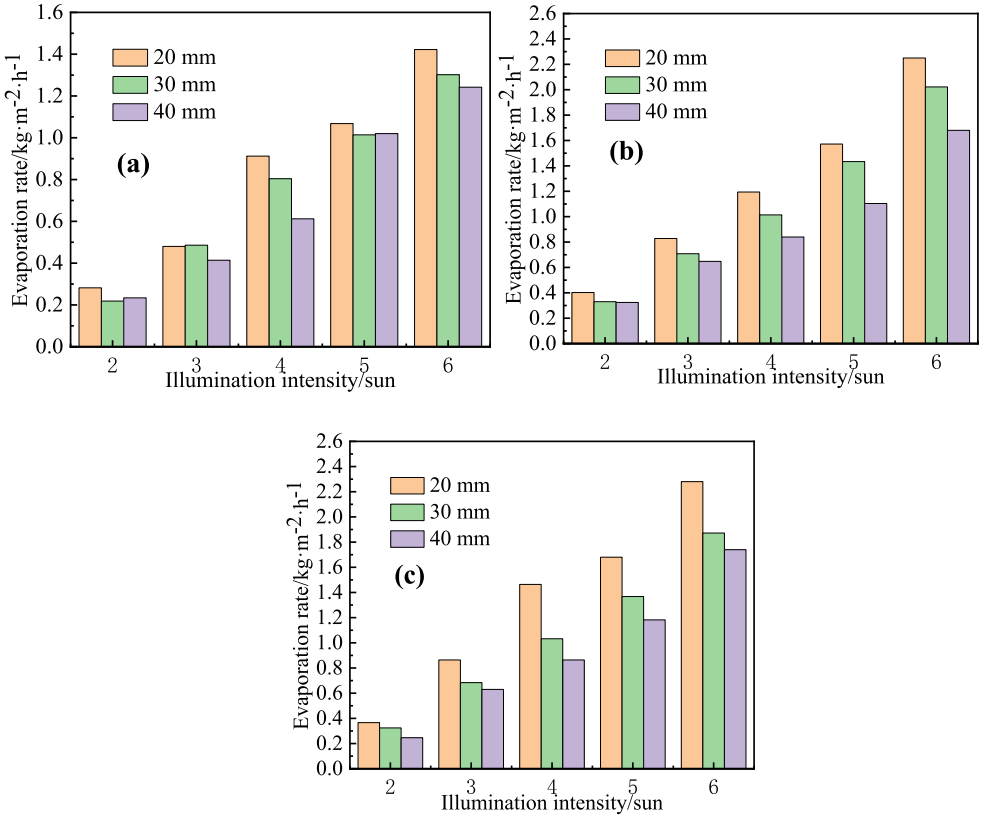

Fig. 8. Evaporation rate of nanofluids with different mass fractions. (a) 50 ppm, (b) 100 ppm, (c) 150 ppm.

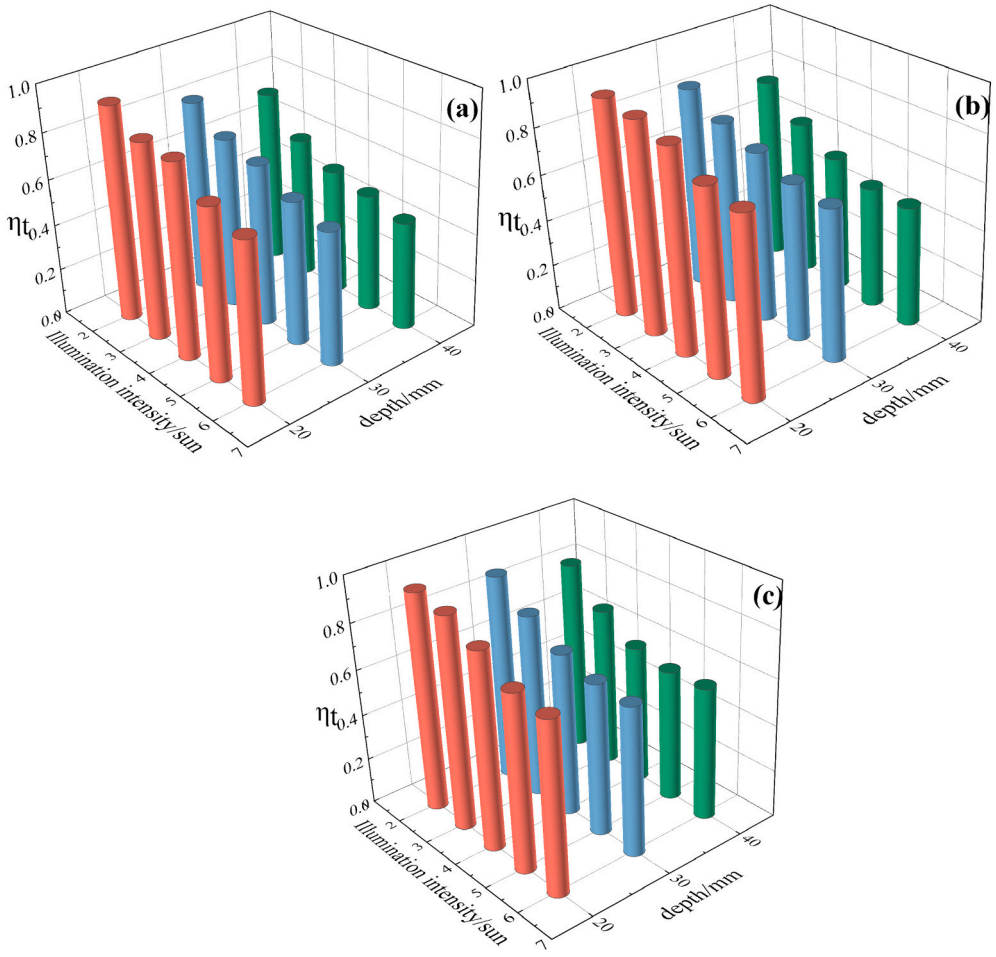

Fig. 9. Heat collection efficiency of nanofluids with different mass fractions. (a) 50 ppm, (b) 100 ppm, (c) 150 ppm.

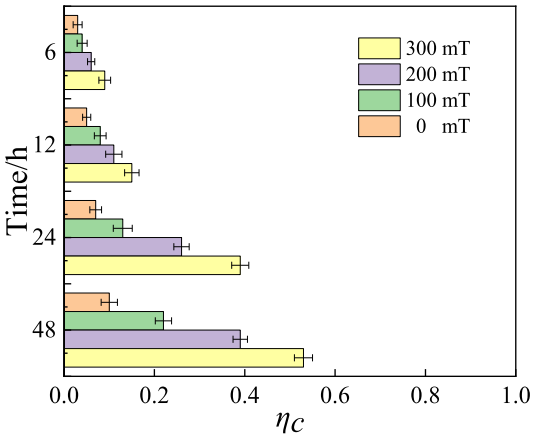

Fig. 10. Variation of recovery efficiency with the magnetic field.

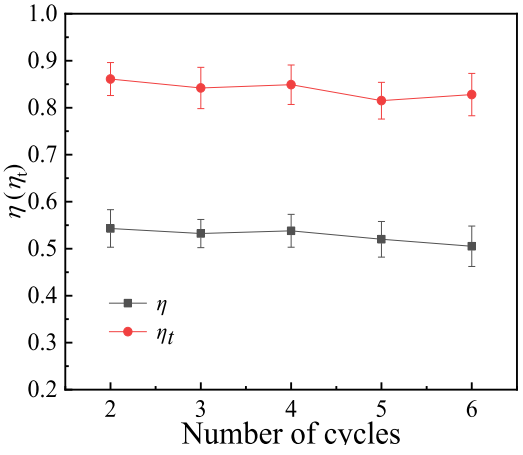

Fig. 11. Variation of efficiency with the number of cycles.

depth makes the upper nanofluids and the lower nanofluids proceed by heat conduction and micro-convection, which causes heat transfer losses and thus reduces the collector efficiency.

3.4. Recovery and recycling

Common photothermal materials are often costly, and in order to increase the recycling of photothermal materials, this section discusses the effect of different magnetic field strengths on nanoparticle recycling efficiency and the variation of photothermal efficiency with the number of cycles. In this work, the recovery efficiency under normal room temperature and sunlight conditions is investigated when the nanofluids concentration is 100 ppm. Fig. 10 shows the recovery efficiency of nanoparticles under different magnetic field conditions. It can be seen that when the magnetic field strength is 300 mT, the recovery of nanoparticles can reach 53%, which is 42% better than no magnetic field. Similarly, the recycling efficiency of nanofluids with a mass

fraction of 100 ppm under the condition of 2 sun light intensity and 20 mm depth is investigated. Fig. 11 shows the variation of the photothermal efficiency with different numbers of cycles. It is clear to see that after cycling the nanoparticles 6 times, the heating efficiency and heat collection efficiency slightly decreases, but the decrease was not significant, with excellent scope for recycling.

4. Conclusions

Functionalized carbon nanotubes loaded with Fe_3O_4 were prepared and morphological and optical properties were characterized. The photothermal and recovery properties of Fe_3O_4/CNTs nanofluids in DASC were investigated. Some of the main findings are as follows:

(1) The heat collection efficiency of the collector increases with the concentration of the nanofluids. However, increasing the concentration of nanofluids does not always increase the collector efficiency significantly. When the nanofluids concentration is 100 ppm, the collector efficiency can reach 94.14%.
(2) The increase in nanofluids' depth increases the heat loss inside the collector, leading to a decrease in collector efficiency. In this experiment, the nanofluids depth of 20 mm showed the best photothermal performance.
(3) Fe_3O_4/CNTs with magnetic properties show excellent recyclable performance under the action of the magnetic field, and the recycling efficiency can reach 53% at the magnetic field strength of 300 mT, while the nanofluids can maintain stable photothermal performance after several cycles.

CRediT authorship contribution statement

Zhibo Tang: Writing – original draft, Writing – review & editing, Investigation. **Lanqi Chen:** Investigation, Writing – review & editing. **Cong Qi:** Conceptualization, Methodology, Investigation, Writing – review & editing. **Zhen Tian:** Writing – review & editing.

Declaration of Competing Interest

The authors declare that they have no known competing financial interests or personal relationships that could have appeared to influence the work reported in this paper.

Acknowledgements

This work is financially supported by “Natural Science Foundation of Jiangsu Province, China” (Grant No. BK20181359).

References

[1] A. Lingayat, R. Balijepalli, V.P. Chandramohan, Applications of solar energy based drying technologies in various industries-a review, Sol. Energy 229 (2021) 52–68.
[2] G. Hu, X. Ning, M. Hussain, U. Sajjad, M. Sultan, H.M. Ali, T.R. Shah, H. Ahmad, Potential evaluation of hybrid nanofluids for solar thermal energy harvesting: a review of recent advances, Sustain Energy Techn. 48 (2021), 101651.
[3] M. Bahiraei, M. Hangi, Flow and heat transfer characteristics of magnetic nanofluids: a review, J. Magn. Magn. Mater. 374 (2015) 125–138.
[4] M.H. Esfe, M.K. Amiri, M. Bahiraei, Optimizing thermophysical properties of nanofluids using response surface methodology and particle swarm optimization in a non-dominated sorting genetic algorithm, J. Taiwan Inst. Chem. E 103 (2019) 7–19.
[5] M. Pavia, K. Alajami, P. Estelle, A. Desforges, B. Vigolo, A critical review on thermal conductivity enhancement of graphene-based nanofluids, Adv. Colloid Interf. Sci. 294 (2021), 102452.
[6] W. Cui, Z. Cao, X. Li, L. Lu, T. Ma, Q. Wang, Experimental investigation and artificial intelligent estimation of thermal conductivity of nanofluids with different nanoparticles shapes, Powder Technol. 398 (2022), 117078.
[7] A. Barkhordar, R. Ghasemiasl, T. Armaghani, Statistical study and a complete overview of nanofluid viscosity correlations: a new look, J. Therm. Anal. Calorim. (2021), https://doi.org/10.1007/s10973-021-10993-y.
[8] C. Cheng, M. Zhang, S. Wang, Y. Li, H. Feng, D. Bu, Z. Xu, Y. Liu, L. Jin, L. Xiao, Y. Ao, Improving interfacial properties and thermal conductivity of carbon fiber/epoxy composites via the solvent-free GO@Fe_3O_4 nanofluid modified water-based sizing agent, Compos. Sci. Technol. 209 (2021), 108788.
[9] N. Abu-Libdeh, F. Redouane, A. Aissa, F. Mebarek-Oudina, A. Almuhtady, W. Jamshed, W. Al-Kouz, Hydrothermal and entropy investigation of Ag/MgO/H_2O hybrid nanofluid natural convection in a novel shape of porous cavity, Appl. Sci. 11 (4) (2021) 1722.
[10] S. Goudarzi, M. Shekaramiz, A. Omidvar, E. Golab, A. Karimipour, A. Karimipour, Nanoparticles migration due to thermophoresis and Brownian motion and its impact on Ag-MgO/water hybrid nanofluid natural convection, Powder Technol. 375 (2020) 493–503.
[11] M.E. Haque, M.S. Hossain, H.M. Ali, Laminar forced convection heat transfer of nanofluids inside non-circular ducts: a review, Powder Technol. 378 (2021) 808–830.
[12] M. Bahiraei, M. Naseri, A. Monavari, Thermal-hydraulic performance of a nanofluid in a shell-and-tube heat exchanger equipped with new trapezoidal inclined baffles: nanoparticle shape effect, Powder Technol. 395 (2022) 348–359.
[13] S. Mukherjee, S. Ebrahim, P.C. Mishra, N. Ali, P. Chaudhuri, A review on pool and flow boiling enhancement using nanofluids: nuclear reactor application, Processes 10 (1) (2022) 177.
[14] X. Ma, Y. Song, Y. Wang, Y. Zhang, J. Xu, S. Yao, K. Vafai, Experimental study of boiling heat transfer for a novel type of GNP-Fe_3O_4 hybrid nanofluids blended with different nanoparticles, Powder Technol. 396 (2022) 92–112.
[15] X. Wang, L. Luo, J. Xiang, S. Zheng, S. Shittu, Z. Wang, X. Zhao, A comprehensive review on the application of nanofluid in heat pipe based on the machine learning: theory, application and prediction, Renew. Sust. Energ. Rev. 150 (2021), 111434.
[16] H. Ghorabaee, M.R.S. Emami, F. Moosakazemi, N. Karimi, G. Cheraghian, M. Afrand, The use of nanofluids in thermosyphon heat pipe: a comprehensive review, Powder Technol. 394 (2021) 250–269.
[17] M. Jamshidmofid, M. Bahiraei, Thermohydraulic assessment of a novel hybrid nanofluid containing cobalt oxide-decorated reduced graphene oxide nanocomposite in a microchannel heat sink with sinusoidal cavities and rectangular ribs, Int. Commun. Heat Mass Transf. 131 (2022), 105769.
[18] J. Tu, C. Qi, K. Li, Z. Tang, Numerical analysis of flow and heat characteristic around micro-ribbed tube in heat exchanger system, Powder Technol. 395 (2022) 562–583.
[19] Z. Li, A. Kan, K. Wang, Y. He, N. Zheng, W. Yu, Optical properties and photothermal conversion performances of graphene based nanofluids, Appl. Therm. Eng. 203 (2022), 117948.
[20] M. Chen, Y. He, J. Zhu, Y. Shuai, B. Jiang, Y. Huang, An experimental investigation on sunlight absorption characteristics of silver nanofluids, Sol. Energy 115 (2015) 85–94.
[21] M. Chen, Y. He, J. Zhu, D. Wen, Investigating the collector efficiency of silver nanofluids based direct absorption solar collectors, Appl. Energy 181 (2016) 65–74.
[22] J. Jeon, S. Park, B.J. Lee, Optical property of blended plasmonic nanofluid based on gold nanorods, Opt. Express 22 (104) (2014) A1101–A1111.
[23] X. Yu, Y. Zhong, Y. Sun, Y. Chen, Controllable preparation of plasmonic gold nanostars for enhanced photothermal and SERS effects, Chem. Res. Chin. Univ. 36 (6) (2020) 1284–1291.
[24] Y. Xuan, H. Duan, Q. Li, Enhancement of solar energy absorption using a plasmonic nanofluid based on TiO_2/Ag composite nanoparticles, RSC Adv. 4 (31) (2014) 16206–16213.
[25] H. Li, Y. He, Z. Liu, Y. Huang, B. Jiang, Synchronous steam generation and heat collection in a broadband Ag@TiO_2 core-shell nanoparticle-based receiver, Appl. Therm. Eng. 121 (2017) 617–627.
[26] H. Li, Y. He, Z. Liu, B. Jiang, Y. Huang, Rapid synthesis of broadband Ag@TiO_2 core-shell nanoparticles for solar energy conversion, Sol. Energ. Mat. Sol. C. 166 (2017) 52–60.
[27] H. Li, Y. He, C. Wang, X. Wang, Y. Hu, Tunable thermal and electricity generation enabled by spectrally selective absorption nanoparticles for photovoltaic/thermal applications, Appl. Energy 236 (2019) 117–126.
[28] J. Huang, Y. He, M. Chen, B. Jiang, Y. Huang, Solar evaporation enhancement by a compound film based on au@TiO_2 core-shell nanoparticles, Sol. Energy 155 (2017) 1225–1232.
[29] Q. Zhang, W. Xu, X. Wang, Carbon nanocomposites with high photothermal conversion efficiency, Sci. China Mater. 61 (7) (2018) 905–914.
[30] S.M. Ladjevardi, A. Asnaghi, P.S. Izadkhast, A.H. Kashani, Applicability of graphite nanofluids in direct solar energy absorption, Sol. Energy 94 (2013) 327–334.
[31] S. Delfani, M. Karami, M.A.A. Behabadi, Performance characteristics of a residential-type direct absorption solar collector using MWCNT nanofluid, Renew. Energy 87 (2016) 754–764.
[32] L. Zhang, J. Liu, G. He, Z. Ye, X. Fang, Z. Zhang, Radiative properties of ionic liquid-based nanofluids for medium-to-high-temperature direct absorption solar collectors, Sol. Energ. Mat. Sol. C. 130 (2014) 521–528.
[33] E. Sani, L. Mercatelli, S. Barison, C. Pagura, F. Agresti, L. Colla, P. Sansoni, Potential of carbon nanohorn-based suspensions for solar thermal collectors, Sol. Energ. Mat. Sol. C. 95 (11) (2011) 2994–3000.
[34] M. Karami, M.A. Akhavan Bahabadi, S. Delfani, A. Ghozatloo, A new application of carbon nanotubes nanofluid as working fluid of low-temperature direct absorption solar collector, Sol. Energ. Mat. Sol. C. 121 (2014) 114–118.
[35] L. Chen, J. Liu, X. Fang, Z. Zhang, Reduced graphene oxide dispersed nanofluids with improved photo-thermal conversion performance for direct absorption solar collectors, Sol. Energ. Mat. Sol. C. 163 (2017) 125–133.
[36] N. Hordy, D. Rabilloud, J.L. Meunier, S. Coulombe, High temperature and long-term stability of carbon nanotube nanofluids for direct absorption solar thermal collectors, Sol. Energy 105 (2014) 82–90.

[37] W. Chen, C. Zou, X. Li, An investigation into the thermophysical and optical properties of SiC/ionic liquid nanofluid for direct absorption solar collector, Sol. Energ. Mat. Sol. C. 163 (2017) 157–163.
[38] T.B. Gorji, A.A. Ranjbar, A numerical and experimental investigation on the performance of a low-flux direct absorption solar collector (DASC) using graphite, magnetite and silver nanofluids, Sol. Energy 135 (2016) 493–505.
[39] X. Li, C. Zou, W. Chen, X. Lei, Experimental investigation of β-cyclodextrin modified carbon nanotubes nanofluids for solar energy systems: stability, optical properties and thermal conductivity, Sol. Energ. Mat. Sol. C. 157 (2016) 572–579.
[40] J. Liu, C. Xu, L. Chen, X. Fang, Z. Zhang, Preparation and photo-thermal conversion performance of modified graphene/ionic liquid nanofluids with excellent dispersion stability, Sol. Energ. Mat. Sol. C. 170 (2017) 219–232.
[41] A. Mashhadian, M.M. Heyhat, O. Mahian, Improving environmental performance of a direct absorption parabolic trough collector by using hybrid nanofluids, Energy Convers. Manag. 244 (2021), 114450.
[42] P.G. Struchalin, D.M. Kuzmenkov, V.S. Yunin, X. Wang, Y. He, B.V. Balakin, Hybrid nanofluid in a direct absorption solar collector: magnetite vs. carbon nanotubes compete for thermal performance, Energies 15 (5) (2022) 1604.
[43] S. Delfani, M. Karami, M.A. Akhavan-Behabadi, Performance characteristics of a residential-type direct absorption solar collector using MWCNT nanofluid, Renew. Energy 87 (2016) 754–764.
[44] Y. Tong, J. Kim, H. Cho, Effects of thermal performance of enclosed-type evacuated U-tube solar collector with multi-walled carbon nanotube/water nanofluid, Renew. Energy 83 (2015) 463–473.
[45] A. Kasaeian, R. Daneshazarian, R. Rezaei, F. Pourfayaz, G. Kasaeian, Experimental investigation on the thermal behavior of nanofluid direct absorption in a trough collector, J. Clean. Prod. 158 (2017) 276–284.
[46] Y. He, M. Chen, X. Wang, Y. Hu, Plasmonic multi-thorny gold nanostructures for enhanced solar thermal conversion, Sol. Energy 171 (2018) 73–82.
[47] M. Chen, Y. He, J. Zhu, Preparation of Au-Ag bimetallic nanoparticles for enhanced solar photothermal conversion, Int. J. Heat Mass Transf. 114 (2017) 1098–1104.